

Article

# Hydroformylation of Alkenes over Phosphorous-Free Rhodium Supported on N-Doped Silica

Yulia Kardasheva \*, Maria Terenina , Daniil Sokolov , Natalia Sinikova , Sergey Kardashev   
and Eduard Karakhanov \*

Department of Chemistry, Lomonosov Moscow State University, 119234 Moscow, Russia; tereninam@petrol.chem.msu.ru (M.T.); daniil-01.10@yandex.ru (D.S.); 7422990@mail.ru (N.S.); chemus6@gmail.com (S.K.)

\* Correspondence: yuskard@petrol.chem.msu.ru (Y.K.); karakhanov@petrol.chem.msu.ru (E.K.); Tel.: +7-495-939-1543 (Y.K.)

**Abstract:** A new phosphorous-free rhodium supported on a nitrogen-doped silica was successfully used as a catalyst for the hydroformylation of alkenes. The obtained material and the catalyst were characterized by XRD, XPS, FTIR, SEM, TEM, ICP AES, and low-temperature nitrogen adsorption-desorption measurements. The catalytic performance was studied by the example of the hydroformylation of octene-1 at temperatures of 80–140 °C and a pressure of 5.0 MPa. The catalyst provided a 99% conversion of 1-octene with a 98% yield of aldehydes and showed a good conversion of styrene and cyclohexene. The catalyst can be repeatedly used in ten consecutive cycles, with its activity remaining constant.

**Keywords:** heterogeneous catalysis; olefin hydroformylation; hybrid materials; urea; silica; rhodium



**Citation:** Kardasheva, Y.; Terenina, M.; Sokolov, D.; Sinikova, N.; Kardashev, S.; Karakhanov, E. Hydroformylation of Alkenes over Phosphorous-Free Rhodium Supported on N-Doped Silica. *Catalysts* **2023**, *13*, 818. <https://doi.org/10.3390/catal13050818>

Academic Editor: Gang Li

Received: 3 April 2023

Revised: 24 April 2023

Accepted: 27 April 2023

Published: 28 April 2023



**Copyright:** © 2023 by the authors. Licensee MDPI, Basel, Switzerland. This article is an open access article distributed under the terms and conditions of the Creative Commons Attribution (CC BY) license (<https://creativecommons.org/licenses/by/4.0/>).

## 1. Introduction

Hydroformylation (oxo process), discovered by Otto Roelen as far back as 1938, is still widely used to produce aldehydes, which can further be converted into alcohols, ethers and esters, carboxylic acids, aliphatic amines, and other derivatives with high added value [1]. The modern industrial hydroformylation process is based on homogeneous rhodium systems [2–5]. However, one of the main problems of homogeneous hydroformylation has long been the difficulty of the recovery of the catalyst from the reaction mixture and the purification of the catalyst. These stages are inevitably accompanied by a loss of rhodium, which significantly increases the cost of the process. Over recent decades, much effort has been made to solve this problem, and various approaches have been developed for the recovery of soluble rhodium catalysts, such as performing the reaction in “unconventional” solvents (ionic liquids, water, and fluorinated and supercritical solvents) [6–9], as well as using catalysts supported on various supports (silica, zeolites, polymers, carbon materials, etc.) [10–12]. The use of supported catalysts is considered one of the most available approaches due to their advantages: they are easy to recover by simple methods (filtration, centrifugation, magnetic separation, etc.) and can be reused. Their main disadvantages are the leaching of the metal complex during the reaction (leaching of the metal into the liquid phase), a complex synthesis procedure, and a lower catalyst activity in comparison with homogeneous systems.

To date, rhodium complexes with phosphine ligands are rightfully recognized as the most efficient hydroformylation catalysts [13]; however, their use, in both laboratory practice and industry, is greatly complicated by the extreme sensitivity of the ligand to oxidation. Therefore, along with the problem of recovery from the reaction medium, the question of the search for catalytic systems resistant to oxidative and hydrolytic action remains quite important. In this context, an alternative to phosphine ligands can be

nitrogen-containing compounds capable of complex formation with many transition metals, including rhodium [14,15].

Hybrid organic–inorganic materials are formed from a homogeneous mixture of interpenetrating inorganic and organic components. They are most often produced by mixing organic monomers with inorganic compounds. A combination of organic and inorganic substances makes it possible to obtain a wide range of new hybrid materials, the properties and applications of which will depend on the raw materials used in the synthesis [16–18]. In particular, they can be used as an efficient solid substrate (support) for metal immobilization due to the presence of complexing groups in the structure of the support [19–21].

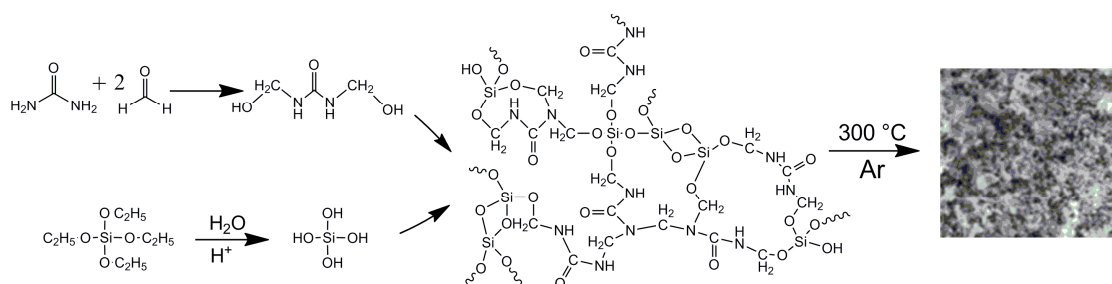
N-doped composite organosilicon materials form covalent bonds with catalytic active metals, which in turn can increase catalyst stability and prevent metal leaching [22–24]. Metal complexes deposited on such supports are quantitatively recovered from the reaction medium and can be reused.

Here, a new hybrid composite based on nitrogen-doped silica was synthesized by the co-condensation of tetraethyl orthosilicate (TEOS) and an organic prepolymer, a product of the condensation of urea and formaldehyde. To obtain a phosphorous-free rhodium catalyst on its basis, a simple and efficient method was proposed, which is based on the formation of a rhodium carbonyl complex by the direct interaction of rhodium trichloride, carbon monoxide, and complexing fragments of the support. For comparison, a rhodium catalyst impregnated into a matrix of nitrogen-free amorphous silica gel (SiO<sub>2</sub>) was prepared by the same method. Both catalysts were tested in the hydroformylation of 1-octene.

## 2. Results and Discussion

### 2.1. Synthesis and Characterization of Supports and Catalysts

The procedure for the synthesis of the composite material comprises TEOS hydrolysis, the primary condensation of urea with formaldehyde to form methylolurea, and the subsequent co-polycondensation of the obtained derivatives (Scheme 1). Further heat treatment of the produced composite (300 °C, Ar) is accompanied by typical reactions of the carbonization process, such as cyclization and condensation, resulting in the formation of a hybrid organic–inorganic material UFSi, the elemental composition of which is presented in Table 1.



**Scheme 1.** Scheme of synthesis of the UFSi composite material.

**Table 1.** Results of analysis of the UFSi composite material.

Contents of Elements in Samples									
EDS Data (wt%)					XPS Data (at.%)				
C	H	N	Si	O	C	N	Si	O	
10.4	1.0	3.5	31.4	53.7	6.4	2.4	33.9	57.3	

The overview XPS spectrum of the obtained material (Figure 1a, Table 2) shows lines of silicon, oxygen, nitrogen, and carbon. The high-resolution spectra of the element lines were decomposed into components (Figure 1b,c, Table 2). The interpretation was based on the published data [25,26].

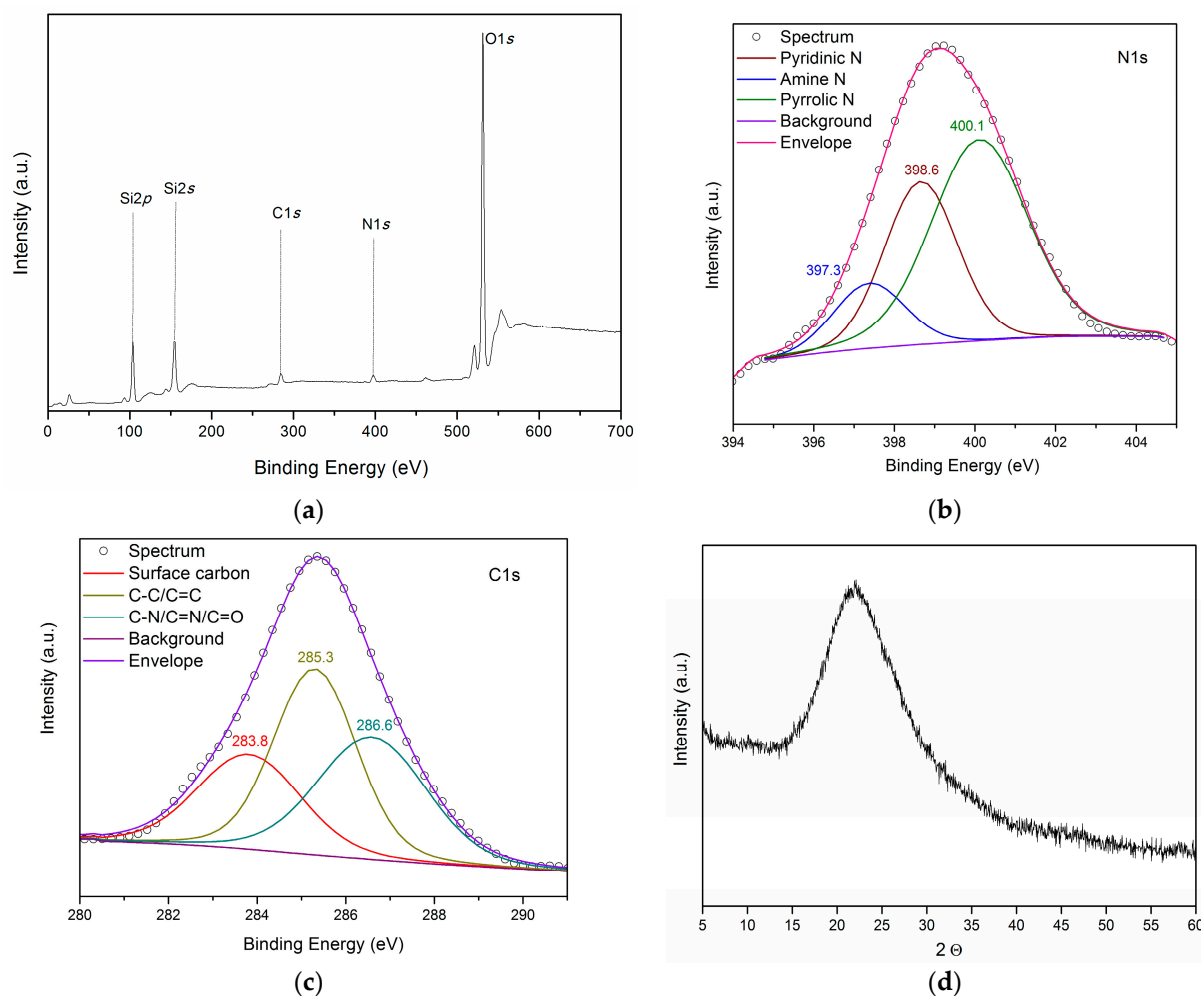


**Figure 1.** (a) XPS survey spectra, (b) N1s and (c) C1s high-resolution XPS spectra, and (d) XRD pattern of UFSi.

**Table 2.** Binding energies and fractions of components in XPS spectra, and the corresponding types of bonds in UFSi.

Core Level	Binding Energy (eV)	Concentration (at.%)	Electron State
N1s	397.4	12.9	C <sub>2</sub> NH, secondary amine
	398.6	32.6	C = N–C, pyridinic-N
	400.1	54.5	N–C, pyrrolic N
C1s	283.8	25.4	Graphite carbon/surface carbon
	285.3	40.0	C–C/C = C ( <i>sp</i> <sup>3</sup> )
	286.6	34.6	C–N/C = N/C = O

The data presented suggest that nitrogen on the surface is present in the composition of pyrrole (400.1 eV), pyridine (398.6 eV), and secondary amine functional groups (397.4 eV) [25–27]. The C1s XPS spectrum is approximated by the sum of three components with maxima at 283.8, 285.3, and 286.2 eV, which can be assigned to atoms of graphitized carbon (25%) and carbon in C–C/C = C (40%) and C–N/C = N/C = O (35%) bonds [25,27].

The XRD pattern of the obtained sample is a wide halo (Figure 1d), indicating an amorphous structure.

The SEM study (Figure 2a) showed that the material has a homogeneous porous structure, which, according to TEM data (Figure 2b), is formed by agglomerates of particles with a size of about 5 nm.

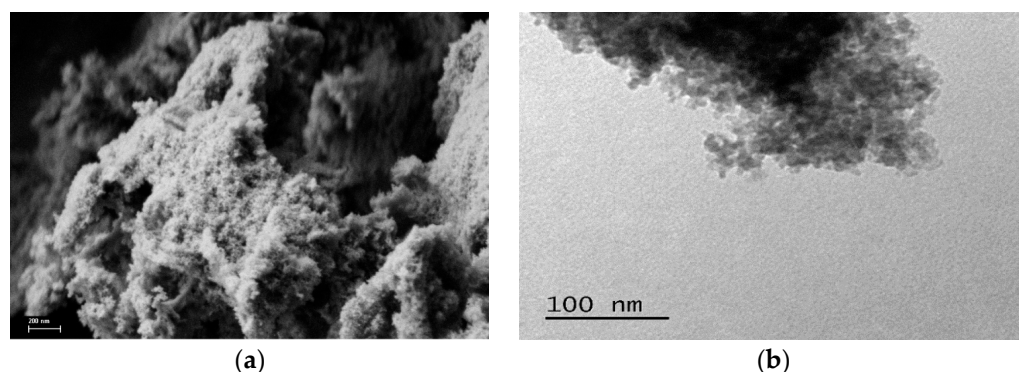


**Figure 2.** SEM (a) and TEM (b) images of UFSi.

The isotherm of low-temperature nitrogen adsorption–desorption for the synthesized composite belongs to type IV according to the IUPAC classification, which is inherent in mesoporous materials. At high relative pressures, the isotherm has a rather steep rise, which is typical of materials with near-cylindrical open mesopores (Figure 3). The surface area calculated by the BET method was  $306 \text{ m}^2/\text{g}$ , and the average pore diameter was  $7.6 \text{ nm}$ .

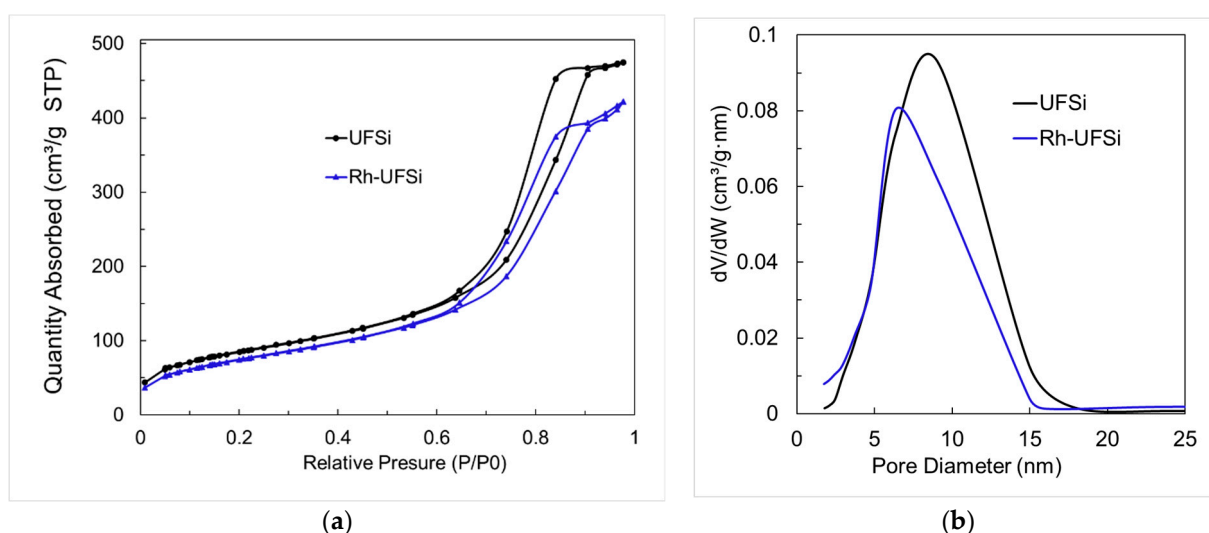


**Figure 3.** (a)  $\text{N}_2$  desorption isotherm curves and (b) pore size distributions of UFSi and Rh-UFSi.

The catalyst was obtained by impregnating the support with rhodium trichloride at an elevated pressure of carbon monoxide at a temperature of  $100 \text{ }^\circ\text{C}$ . The catalyst was supported on either the UFSi composite material (Rh-UFSi catalyst), or an amorphous silica sample that had similar textural characteristics but was not doped with nitrogen (Rh-Si catalyst).

The data of low-temperature nitrogen adsorption–desorption (Figure 3, Table 3) show that there was no significant decrease in the surface area and pore size of the support during the deposition of rhodium.

**Table 3.** Textural parameters of UFSi and Rh-UFSi.

Sample	Rh (wt%)	Surface Area ( $\text{m}^2/\text{g}$ )	Pore Size (nm)	Pore Volume ( $\text{cm}^3/\text{g}$ )
UFSi	-	306	7.6	0.73
Rh-UFSi	3.14	272	7.3	0.64

Figure 4 presents the IR spectra of the  $\text{SiO}_2$  and UFSi supports and the Rh-UFSi and Rh-Si catalysts, both fresh and after use in ten and three cycles.

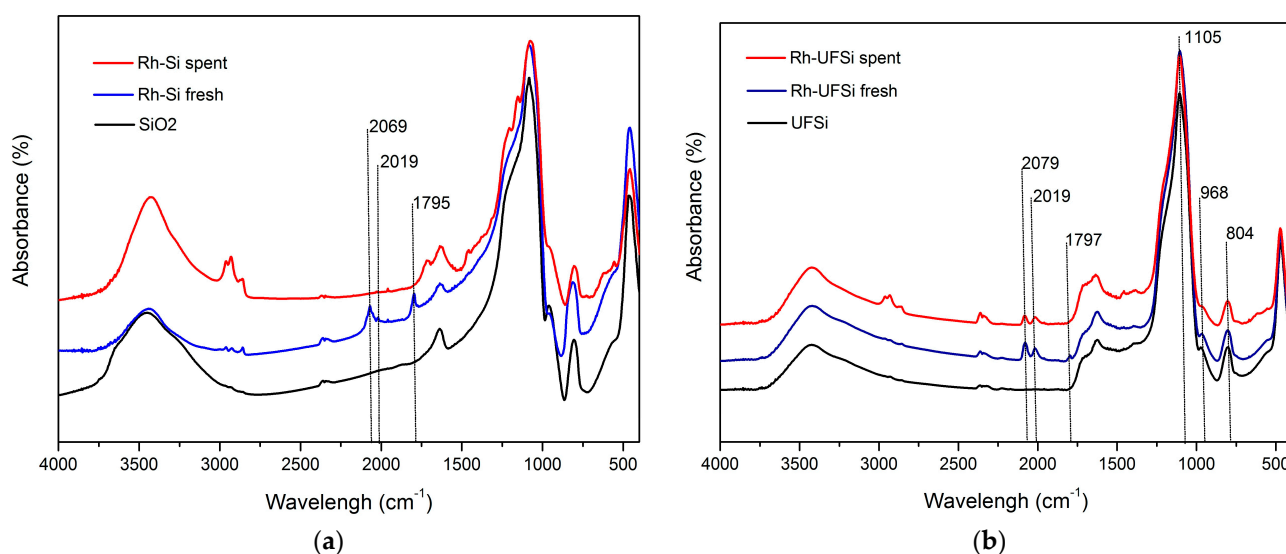


**Figure 4.** IR-spectra of (a) Rh-Si and (b) Rh-UFSi.

The IR spectrum of the UFSi material shows the absorption bands of the stretching vibrations of siloxane Si–O–Si bonds ( $1105\text{ cm}^{-1}$ ) and the bending vibrations of Si–OH bonds ( $968\text{ cm}^{-1}$ ) and Si–O bonds in tetrahedral  $\text{SiO}_4$  fragments ( $804\text{ cm}^{-1}$ ); the multiplet band of medium intensity in the range  $1590\text{--}1750\text{ cm}^{-1}$  can be assigned to the combined frequencies of the skeletal vibrations of N–H and C–N bonds in pyrrole and pyridine structural fragments. After the deposition of rhodium, intense signals appear in the IR spectrum of the Rh-UFSi catalyst at  $2019$  and  $2079\text{ cm}^{-1}$ , which are characteristic of carbonyl ligands coordinated to rhodium, and so does a low-intensity band at  $1797\text{ cm}^{-1}$ , which is due to the vibrations of bridging CO groups of carbonyls  $\text{Rh}_2(\text{CO})$  [28,29]. In the IR spectrum of the Rh-Si catalyst obtained using unmodified silica gel, the signals of coordinated carbonyl ligands are represented by a wide diffuse band with a maximum at  $2069\text{ cm}^{-1}$ , but the absorption band at  $1795\text{ cm}^{-1}$  (bridging CO groups) is quite intense. After the catalytic experiments, the absorption bands of coordinated carbonyl ligands in the spectrum of the Rh-Si sample are not observed. The disappearance of signals from coordinated carbonyl ligands in the spectrum of the spent Rh-Si catalyst sample is indeed associated with the leaching of rhodium carbonyl complexes from the catalyst surface. The hot filtration test carried out by us after the first and second cycles confirmed the activity of the solution in relation to hydroformylation, which indicates that active compounds, apparently rhodium carbonyls, are present in the solution after catalysis. In the spectrum of the spent Rh-UFSi catalyst sample (Figure 4), the signals of only bridging carbonyl ligands ( $1793\text{ cm}^{-1}$ ) disappear, and a couple of bands at  $2019$  and  $2079\text{ cm}^{-1}$  are retained, which indicates the stable anchoring of rhodium carbonyl complexes.

The electronic configurations of rhodium in both catalysts were studied by XPS (Figure 5). For the Rh-Si catalyst, the decomposition of the spectrum in the Rh3d region into components shows that, on the surface, there are both Rh(+1) carbonyl complex compounds (with binding energies of  $308.8$  and  $313.5\text{ eV}$  for Rh3d  $5/2$  and Rh3d  $3/2$ , respectively) and some amount (16%) of Rh(+3) compounds ( $310.2$  and  $314.9\text{ eV}$ ), probably, residual rhodium trichloride [30,31]. For the Rh-UFSi catalyst sample, the spectrum is a doublet of symmetric peaks, the integral intensities of which are in a ratio of 3: 2, and the spin-orbit splitting is  $4.7\text{ eV}$ . The electron binding energies of Rh3d are  $307.8$  and  $312.5\text{ eV}$  for Rh3d  $5/2$  and Rh3d  $3/2$ , respectively, which indicates that Rh is in the +1 oxidation state in the composition of complex compounds with carbonyl ligands and nitrogen complexing groups in the support. An indirect confirmation of the coordination of rhodium to donor nitrogen sites can be the fact that the binding energies for the Rh-UFSi sample turned out to be slightly lower than for Rh-Si.

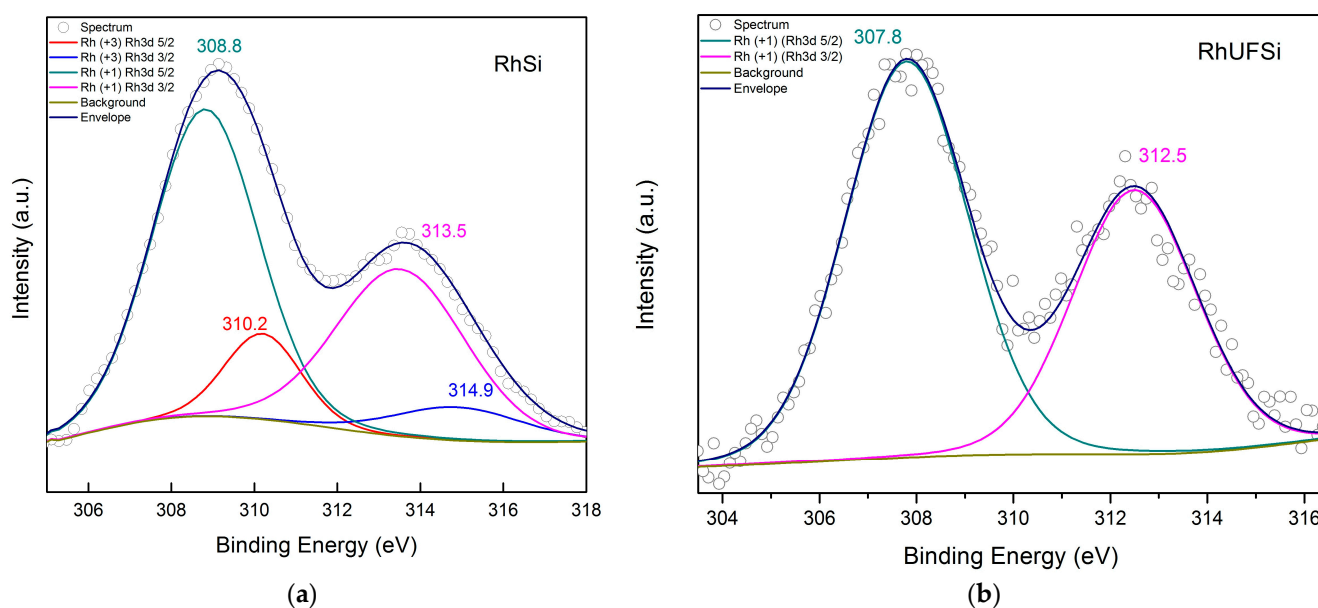
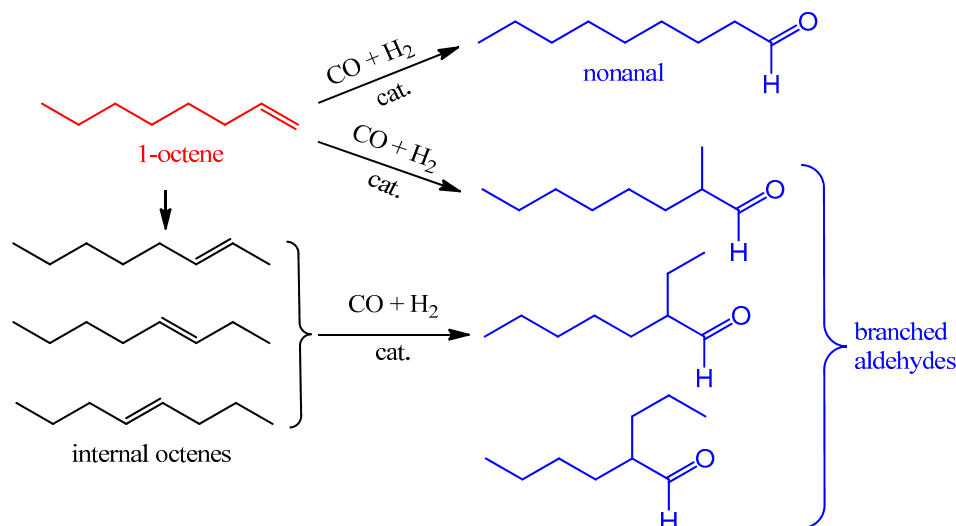


**Figure 5.** High-resolution Rh3d XPS spectra of (a) Rh-Si and (b) Rh-UFSi.

## 2.2. Catalytic Activity

1-Octene was chosen as a model substrate for studying the activity of the obtained heterogeneous catalysts in the hydroformylation reaction (Scheme 2). The process was carried out at a synthesis gas ( $\text{CO}:\text{H}_2 = 1:1$ ) pressure of 3.0 and 5.0 MPa in the temperature range 80–140 °C.



**Scheme 2.** Hydroformylation of 1-octene.

Table 4 shows that the rate of conversion of the initial substrate increases significantly with an increase in temperature from 80 to 100 °C; however, simultaneously, there is also a decrease in the ratio of yields of aldehydes with a linear and isomerized carbon chain (l/b ratio) because of an increase in the yield of the latter, which is explained by the acceleration of both the isomerization of the position of the double bond of 1-octene and the hydroformylation of internal alkenes. With a further increase in temperature, the fraction of isomerized products still somewhat increases, the l/b ratio decreases from 0.7 at 100 °C to 0.5 at 140 °C (Table 4).

**Table 4.** Hydroformylation of 1-octene over the Rh-UFSi catalyst.

Entry	Temperature (°C)	Time (h)	Conversion (%)	Yield of Aldehydes (%)	I/b Ratio
1	80	5	48	32	2.2
2	80	20	95	94	0.9
3	100	2	63	23	2.2
4	100	5	97	79	1.0
5	100	20	99	98	0.7
6	120	2	87	57	0.6
7	120	5	94	84	0.6
8 <sup>1</sup>	120	5	98	64	0.8
9 <sup>2</sup>	120	5	98	53	0.6
10	140	1	87	57	0.6
11	140	2	99	75	0.6
12	140	5	99	96	0.5

Reaction conditions: 0.01 g of catalyst, 2 mL of toluene, 0.3 mL of 1-octene, CO:H<sub>2</sub> = 1, and  $p = 5.0$  MPa. <sup>1</sup> 1 mL of 1-octene. <sup>2</sup>  $p = 3.0$  MPa.

A decrease in the synthesis gas pressure to 3 MPa expectedly leads to a decrease in the yield of aldehydes, whereas the fraction of internal alkenes in the mixture increases (Table 4, entry 9), which can be explained by the slowing down of CO coordination and incorporation during the formation of the acyl intermediate with a decrease in the partial pressure and, consequently, the concentration of carbon monoxide in the reaction medium, which promotes the isomerization reaction at the position of the olefin double bond.

An analysis of the changes in the composition of the reaction mixture, depending on the conversion of 1-octene and the reaction time at a temperature of 100 °C and a synthesis gas pressure of 5 MPa (Figure 6), showed that, early in the process, n-nonanal and 2-methyloctanal are relatively rapidly formed, with the yield of the linear aldehyde being twice as high. Simultaneously, a side process of isomerization of the substrate occurs to form a mixture of internal alkenes, which enter into the hydroformylation reaction much more slowly.

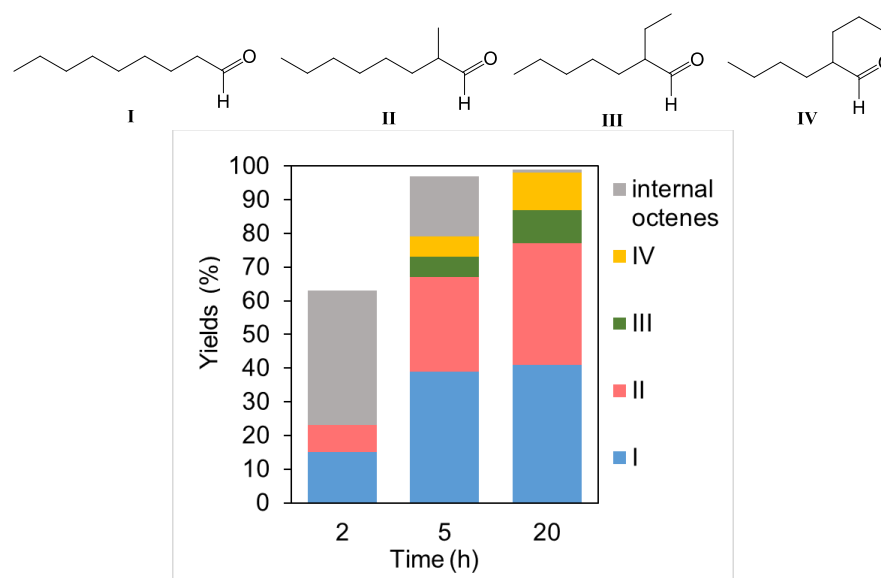


**Figure 6.** Hydroformylation of 1-octene in the presence of the Rh-UFSi catalyst (reaction conditions: 0.01 g of catalyst, 2 mL of toluene, 0.3 mL of 1-octene, CO:H<sub>2</sub> = 1,  $p = 5.0$  MPa, and  $T = 100$  °C).

An increase in the reaction time makes it possible to achieve a quantitative conversion of the alkene into a mixture of aldehydes; notably, 2-ethylheptanal (III) and 2-propylhexanal (IV) are formed in approximately equal amounts, regardless of the conditions (temperature, time, and pressure).

The isomerizing ability of the support was studied in experiments where it was used as a catalyst (Table 5, entry 1), and the contribution of the thermal component to the isomerization was estimated by performing the reaction in an inert gas atmosphere (Table 5, entry 2). In both cases, no 1-octene isomerization was observed at 140 °C for 5 h, which indicates that this process occurs with the participation of the Rh-UFSi catalyst both under hydroformylation conditions and in a hydrogen atmosphere.

**Table 5.** 1-Octene conversion depending on gas composition.

Entry	Catalyst	Gas Composition	Conversion (%)	Yields (%)			
				Octane	Internal Octenes	Branched Aldehydes	Nonanal
1	UFSi	CO:H <sub>2</sub> = 1	0	-	-	-	-
2	Rh-UFSi	Ar	0	-	-	-	-
3	Rh-UFSi	CO:H <sub>2</sub> = 1:2	93	6	78	3	6
4	Rh-UFSi	CO:H <sub>2</sub> = 2:1	100	-	10	57	29
5	Rh-UFSi	H <sub>2</sub>	86	6	80	-	-

Reaction conditions: 0.01 g of catalyst, 2 mL of toluene, 0.3 mL of 1-octene,  $p = 5.0$  MPa,  $T = 140$  °C, and 5 h.

Note that the Rh-UFSi catalyst shows virtually no activity in the hydrogenation of the double bond: the yield of octane did not exceed 6% even when the reaction was carried out in an atmosphere of pure hydrogen (Table 5, entry 5). Enrichment of the CO + H<sub>2</sub> gas mixture with hydrogen to a ratio of 1:2 leads to the inhibition of the hydroformylation, and the main products are internal octenes (Table 5, entry 3). An increase in the partial pressure of carbon monoxide (up to CO:H<sub>2</sub> = 2:1) does not have a significant effect, and the yield of aldehydes slightly decreases, while the n-/iso- ratio remains the same. These results are consistent with the published characteristics of homogeneous hydroformylations in the presence of rhodium complexes with organophosphorus ligands [32]: an increase in the hydrogen partial pressure promotes the formation of hydride complexes responsible for the isomerization. An increase in the substrate/catalyst ratio slows down the hydroformylation, which may be due to the difficulty of carbon monoxide molecules to access the coordination sphere of rhodium because of an increase in the concentration of olefin (Table 4, entry 8), with the hydroformylation of internal double bonds being inhibited to a greater extent.

The most important characteristics of a heterogeneous catalyst, the stability of operation and the possibility of repeated use, were evaluated in ten consecutive cycles at 120 °C for 2 and 5 h of the reaction. Figure 7 shows that the conversion of the initial substrate and the distribution of the products remain virtually the same, beginning with the third cycle.

Elemental analysis data (Table 6) show that the metal loss for the Rh-UFSi catalyst after ten consecutive 5 h long cycles is only 7% of the initial content. Additionally, to test the leachability of rhodium in the form of soluble carbonyls, experiments on a homogeneous hydroformylation of 1-octene were performed, in which the catalysts were filtered liquids after hydroformylation with certain Rh-UFSi catalysts. The reactions were carried out under the same conditions as those with the heterogeneous catalyst. After the first two cycles, a noticeable activity of the homogeneous solution was observed: the conversion of 1-octene was about 80% in 5 h, and after the third cycle, the conversion of 1-octene did not exceed 10%. The totality of these observations confirms that there is no significant leaching of the active metal, and the developed catalyst is characterized by excellent stability.

The Rh-Si catalyst obtained using silica gel containing no nitrogen component lost activity already after the second cycle, and the main products were internal octenes. After three cycles, 0.19 wt% rhodium remained on the support (Table 6).

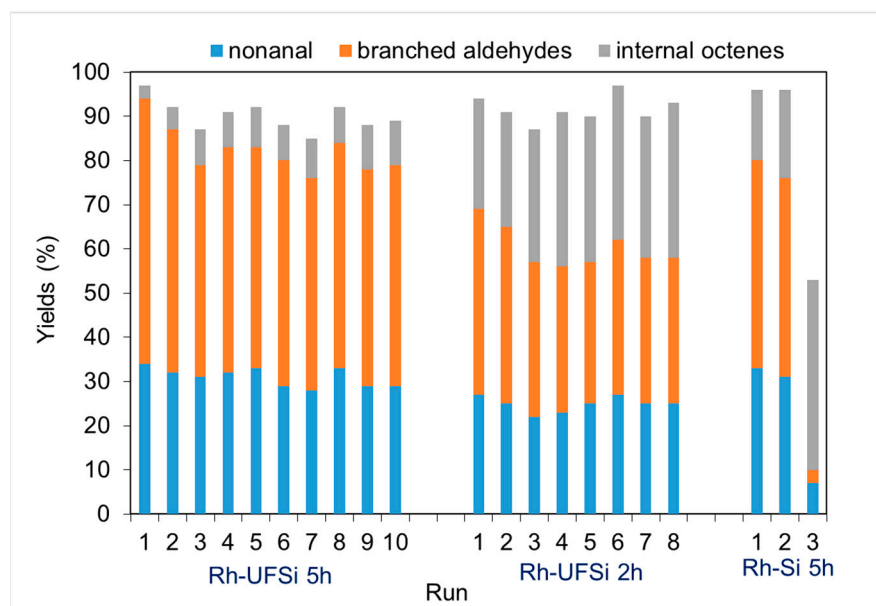


**Figure 7.** Stability test of hydroformylation of 1-octene over the Rh-UFSi and Rh-Si catalysts (reaction conditions: 0.01 g of catalyst, 2 mL of toluene, 0.3 mL of 1-octene,  $\text{CO:H}_2 = 1$ ,  $p = 5.0$  MPa, and  $T = 120$  °C).

**Table 6.** Rhodium content in the Rh-UFSi and Rh-Si catalysts.

Catalyst	Rh Content (wt%)		
	Fresh	Spent	
Rh-UFSi	3.14	2.93 (ten 5 h cycles)	
Rh-Si	4.44	0.19 (three 5 h cycles)	
		3.052 (eight 2 h cycles)	
		—	

Reaction conditions: 0.01 g of catalyst, 2 mL of toluene, 0.3 mL of 1-octene,  $\text{CO:H}_2 = 1$ , and  $p = 5.0$  MPa.

The Rh-UFSi catalyst also showed rather high activity in the hydroformylation of linear alkenes with different chain lengths and structures (styrene and cyclohexene); the results are shown in Table 7. It should be noted that the analysis of the reaction products shows that, in addition to *n*- and isoaldehydes, internal alkenes with double bond shifts are also formed as isomerization byproducts (with the exception of styrene and cyclohexene hydroformylation). The hydrogenation of alkenes to alkanes was not observed. Under the conditions used, neither the yield of aldehydes nor the *n*/*iso* ratio depended on the length of the carbon chain of alkenes. These data are in agreement with the results reported in many articles, for example [33], using Rh nanoparticles.

**Table 7.** Hydroformylation of olefines over the Rh-UFSi catalyst.

Entry	Substrate	Conversion (%)	Yield of Aldehydes (%)	<i>l</i> / <i>b</i> Ratio
1	styrene	48	48	0.6
2	cyclohexene	73	73 <sup>1</sup>	-
3	1-hexene	97	82	1.0
4	1-octene	97	79	1.0
5	1-decene	98	86	0.9
6	1-dodecene	96	84	0.9

Reaction conditions: 0.01 g of catalyst, 2 mL of toluene, 0.002 mol of substrate,  $\text{CO:H}_2 = 1$ , and  $p = 5.0$  MPa.  
<sup>1</sup> 73% cyclohexanal.

The developed Rh-UFSi catalyst showed excellent catalytic characteristics in the hydroformylation of alkenes of various structures, its activity is close to, and in some cases exceeds, the results obtained for catalysts similar in structure presented in the works [34–38].

### 3. Materials and Methods

#### 3.1. Used Reagents

The following reagents were used in this work: methanol CH<sub>3</sub>OH (99%, Acros Organics), sodium hydroxide NaOH (reagent grade, Reakhim, 99%), hydrochloric acid HCl (reagent grade, Irea 2000), tetraethyl orthosilicate TEOS (Sigma-Aldrich, Saint Louis, MO, USA), formaldehyde HCHO (37% aqueous solution, Sigma-Aldrich), urea (99.0%, Component-Reactiv), RhCl<sub>3</sub>·4H<sub>2</sub>O (Aurat), toluene (chemically pure, Component-Reactiv), 1-octene C<sub>8</sub>H<sub>16</sub> (98%, Aldrich), cyclohexene C<sub>6</sub>H<sub>12</sub> (98%, Aldrich), and styrene C<sub>8</sub>H<sub>8</sub> (98%, Aldrich).

Solvents were purified according to standard methods [39].

#### 3.2. Synthesis of the UFSi Support

Solution A: to 20 mL of NaOH solution (pH 8), 4 g (0.07 mol) of urea and 10 mL of 37% formaldehyde solution (0.112 mol) were added, and the obtained mixture was stirred at room temperature for 30 min.

Distilled water (30 mL) and 3.2 mL of 0.2 M HCl solution were mixed in a Teflon liner of a hydrothermal synthesis autoclave at 30 °C. Then, 7 mL of TEOS (0.03 mol) and solution A were successively added while continuously stirring. The mixture was heated to 38–40 °C and stirred for about 10 min, after which the liner was placed in the autoclave, sealed, and kept at a temperature of 100 °C for 24 h. The formed gel was filtered off, washed with distilled water, and dried in air upon heating to 50 °C and then calcined in a muffle furnace in an argon flow at 300 °C for 6 h.

#### 3.3. Synthesis of the Amorphous Support SiO<sub>2</sub>

Distilled water (15 mL) and 1.6 mL of 0.2 M HCl solution were mixed in a Teflon liner of a hydrothermal synthesis autoclave at 30 °C. Then, 3.5 mL of TEOS (0.015 mol) was added dropwise while continuously stirring. The mixture was heated to 38–40 °C and stirred for 10 min, after which the liner was placed in the autoclave, sealed, and kept at a temperature of 100 °C for 24 h. The formed gel was filtered off, washed with distilled water, and dried in air upon heating to 50 °C and then calcined in a muffle furnace in an argon flow at 300 °C for 6 h.

#### 3.4. Preparation of the Catalysts (Rh-UFSi, Rh-Si)

In a steel autoclave, 15 mL of methanol, 25 mg (0.01 mmol) of RhCl<sub>3</sub>·4H<sub>2</sub>O, and 200 mg of the UFSi composite material were placed. The autoclave was sealed, purged three times with carbon monoxide, and then filled with carbon monoxide to a pressure of 3.0 MPa. The autoclave was heated to 100 °C and kept at this temperature while continuously stirring for 24 h. After this time, the autoclave was cooled to room temperature and depressurized, and the precipitate was separated by centrifugation, washed three times with methanol, and dried in a vacuum upon heating to 30 °C. The loading level of Rh in the catalyst before and after the hydroformylation reaction was measured by inductively coupled plasma mass spectrometry (ICP AES). The rhodium content (Rh-UFSi) was 3.14 wt%.

A similar procedure was used to prepare a Rh-Si catalyst on an amorphous SiO<sub>2</sub> support. The rhodium content was 4.44 wt%.

#### 3.5. Characterization

IR spectra were recorded with a Nicolet IR200 spectrometer (Thermo Scientific, Waltham, MA, USA) using KBr pellets with a resolution of 6 cm<sup>-1</sup> in the range 400–4000 cm<sup>-1</sup>. All the spectra were recorded by averaging 100 scans.

Nitrogen adsorption isotherms were measured with a Micromeritics Gemini VII 2390 surface area analyzer (Micromeritics, Norcross, GA, USA). All samples were degassed at 120 °C for 8 h before analysis. The specific surface area SBET was calculated by the Brunauer–Emmett–Teller (BET) method based on adsorption data in a relative pressure range of P/P<sub>0</sub> = 0.05–0.25. The total pore volume V<sub>tot</sub> was determined by the amount of nitrogen adsorbed at a relative pressure of P/P<sub>0</sub> = 0.995.

The morphology and size of the particles were studied by transmission electron microscopy with a JEOL JEM-1011 electron microscope at an accelerating voltage of 100 kV. For each sample, data on 600–1000 particles were processed.

The particle size distribution was determined with a Zetasizer Nano ZS analyzer (Malvern Instruments Ltd., Malvern, Worcestershire, UK) with an integrated 4 mW 633 nm He–Ne laser.

The morphology of the obtained samples was studied by scanning electron microscopy with a Carl Zeiss NVision 40 CrossBeam workstation (magnification to  $9 \times 10^5$ , accelerating voltage 1 kV) in topographic contrast mode. The measurements were performed using the equipment of the Joint Research Center for Physical Methods of Research, Kurnakov Institute of General and Inorganic Chemistry, Russian Academy of Sciences (JRC PMR IGIC RAS).

The quantitative determination of rhodium in the samples was carried out by inductively coupled plasma atomic emission spectroscopy (ICP AES) with an IRIS Intrepid II XDL mass spectrometer (Thermo Electron Corp., Waltham, MA, USA) at a wavelength 343.49 nm.

XPS studies were performed with a LAS-3000 electron spectrometer equipped with an OPX-150 photoelectron retarding potential analyzer (aluminum anode, AlK $\alpha$  radiation 1486.6 eV, tube voltage 12 kV, emission current 20 mA). Photoelectron peaks were calibrated to the carbon C1s peak at 285 eV. XRD was performed with a Rigaku Rotaflex D/max-RC diffractometer (CuK $\alpha$  radiation,  $\lambda = 0.154$  nm,  $2\theta$  range  $3^\circ$ – $50^\circ$ , step  $0.04^\circ$ , scanning rate 4 deg/min). The degree of crystallinity was calculated from the ratio between the areas (integral intensities) of the peaks of the crystalline and amorphous phases.

The percentage of carbon, nitrogen, and hydrogen were determined by elemental analysis on an Elementar vario MICRO cube CHNS analyzer. The samples were burned at 950 °C using helium as a carrier gas (120 mL/min). The products (nitrogen, carbon dioxide, and water) were separated on a thermal desorption column of the analyzer in a helium flow with a thermal conductivity detector.

The reaction mixture was analyzed with a Khromos chromatograph equipped with a flame ionization detector and a 50 m  $\times$  0.2 mm column (DB-5 phase) at a temperature programmed from 60 to 235 °C and a heating rate of 10 deg/min. The carrier gas was helium (30 mL/min). Conversion (%) was determined from changes in the relative peak areas of the substrate and the products.

### 3.6. General Procedure of the Catalytic Experiments

Hydroformylation was carried out in a 25 mL steel autoclave equipped with a magnetic stirrer and a thermostat at a syngas pressure of 3.0–5.0 MPa (CO:H<sub>2</sub> = 1:1) in the temperature range 80–140 °C. The autoclave was loaded with calculated amounts of the catalyst, the substrate, and toluene. The reaction was performed while continuously stirring for a specified time. Then, the autoclave was cooled to room temperature and depressurized. The catalyst was recovered from the reaction solution by centrifugation and then reused in the reaction.

## 4. Conclusions

A mesoporous composite material was synthesized by the hydrothermal method by the co-condensation of a urea–formaldehyde prepolymer and TEOS. The structure and chemical composition of the obtained material were characterized by low-temperature nitrogen adsorption–desorption, IR spectroscopy, XPS, and XRD. A simple and efficient method was proposed for the heterogenization of the hydroformylation catalyst by the preparation of a rhodium carbonyl complex by the direct interaction of rhodium trichloride, carbon monoxide, and complexing fragments of the support. It was shown that the presence of nitrogen-containing functional groups in the composition of the material makes it possible to efficiently anchor rhodium complexes. The developed Rh-UFSi catalyst demonstrates excellent catalytic performance in the hydroformylation of octene, styrene,

and cyclohexane and retains catalytic stability after ten reaction cycles. The proposed catalyst has potential value for engineering applications.

**Author Contributions:** All authors contributed to the study conception and design. Y.K., writing and conceptualization; M.T., methodology; D.S. and N.S., investigation; S.K., formal analysis; E.K., supervision. All authors have read and agreed to the published version of the manuscript.

**Funding:** This study was carried out within the framework of the State Assignment “Petrochemistry and Catalysis. Rational Use of Carbonaceous Raw Materials” (project no. 121031300092-6).

**Data Availability Statement:** All discussed data is inside this article.

**Conflicts of Interest:** The authors declare no conflict of interest.

## References

1. Cornils, B.; Herrmann, W.A.; Rasch, M. Otto Roelen, Pioneer in Industrial Homogeneous Catalysis. *Angew. Chem. Int. Ed. Engl.* **1994**, *33*, 2144–2163. [[CrossRef](#)]
2. Franke, R.; Selent, D.; Börner, A. Applied Hydroformylation. *Chem. Rev.* **2012**, *112*, 5675–5732. [[CrossRef](#)]
3. Tudor, R. Enhancement of Industrial Hydroformylation Processes by the Adoption of Rhodium-Based Catalyst: Part I Development of the LP OXO SM Process to the Commercial Stage. *Platin. Met. Rev.* **2007**, *51*, 116–126. [[CrossRef](#)]
4. Mika, L.T.; Ungváry, F. Hydroformylation—Homogeneous. In *Encyclopedia of Catalysis*; Horváth, I.T., Ed.; John Wiley & Sons, Inc.: Hoboken, NJ, USA, 2011.
5. Medici, S.; Peana, M.; Pelucelli, A.; Zoroddu, M.A. Rh(I) Complexes in Catalysis: A Five-Year Trend. *Molecules* **2021**, *26*, 2553. [[CrossRef](#)]
6. Haumann, M.; Riisager, A. Hydroformylation in Room Temperature Ionic Liquids (RTILs): Catalyst and Process Developments. *Chem. Rev.* **2008**, *108*, 1474–1497. [[CrossRef](#)] [[PubMed](#)]
7. Maqeda, L.; Makhubela, B.C.E.; Smith, G.S. Synthesis, characterization and evaluation of fluorocarbon-containing rhodium(I) complexes for biphasic hydroformylation reactions. *Polyhedron* **2015**, *91*, 128–135. [[CrossRef](#)]
8. Bektsev, S.; Kleman, A.M.; Marteel-Parrish, A.E.; Abraham, M.A. Hydroformylation in supercritical carbon dioxide: Catalysis and benign solvents. *J. Supercrit. Fluids* **2006**, *38*, 232–241. [[CrossRef](#)]
9. De, C.; Saha, R.; Ghosh, S.K.; Ghosh, A.; Mukherjee, K.; Bhattacharyya, S.S.; Saha, B. A review of biphasic hydroformylation for long chain substrates. *Res. Chem. Intermed.* **2013**, *39*, 3463–3474. [[CrossRef](#)]
10. Liu, B.; Wang, Y.; Huang, N.; Lan, X.; Xie, Z.; Chen, J.G.; Wang, T. Heterogeneous hydroformylation of alkenes by Rh-based catalysts. *Chem* **2022**, *8*, 2630–2658. [[CrossRef](#)]
11. Hanf, S.; Alvarado Rupflin, L.; Gläser, R.; Schunk, S.A. Current State of the Art of the Solid Rh-Based Catalyzed Hydroformylation of Short-Chain Olefins. *Catalysts* **2020**, *10*, 510. [[CrossRef](#)]
12. Zhuchkov, D.P.; Nenasheva, M.V.; Terenina, M.V.; Kardasheva, Y.S.; Gorbunov, D.N.; Karakhanov, E.A. Polymeric Heterogeneous Catalysts in the Hydroformylation of Unsaturated Compounds. *Pet. Chem.* **2021**, *61*, 1–14. [[CrossRef](#)]
13. Zhang, B.; Peña Fuentes, D.; Börner, A. Hydroformylation. *ChemTexts* **2021**, *8*, 2. [[CrossRef](#)]
14. Gorbunov, D.N.; Nenasheva, M.V.; Terenina, M.V.; Kardasheva, Y.S.; Naranov, E.R.; Bugaev, A.L.; Soldatov, A.V.; Maximov, A.L.; Tilloy, S.; Monflier, E.; et al. Phosphorus-free nitrogen-containing catalytic systems for hydroformylation and tandem hydroformylation-based reactions. *Appl. Catal. A Gen.* **2022**, *647*, 118891. [[CrossRef](#)]
15. Pombeiro, A.J.L. Nitrogen ligands. *Dalton Trans.* **2019**, *48*, 13904–13906. [[CrossRef](#)] [[PubMed](#)]
16. Bourgeat-Lami, E. Hybrid Organic/Inorganic Particles. In *Hybrid Materials*; Kickelbick, G., Ed.; Wiley-VCH Verlag GmbH & Co. KGaA: Weinheim, Germany, 2006; pp. 87–149.
17. Chujo, Y. Organic–Inorganic hybrid materials. *Curr. Opin. Solid State Mater. Sci.* **1996**, *1*, 806–811. [[CrossRef](#)]
18. Van Der Voort, P.; Esquivel, D.; De Canck, E.; Goethals, F.; Van Driessche, I.; Romero-Salguero, F.J. Periodic Mesoporous Organosilicas: From simple to complex bridges; a comprehensive overview of functions, morphologies and applications. *Chem. Soc. Rev.* **2013**, *42*, 3913–3955. [[CrossRef](#)]
19. Zou, H.; Wu, S.; Shen, J. Polymer/Silica Nanocomposites: Preparation, Characterization, Properties, and Applications. *Chem. Rev.* **2008**, *108*, 3893–3957. [[CrossRef](#)] [[PubMed](#)]
20. Soler-Illia, G.J.A.A.; Azzaroni, O. Multifunctional hybrids by combining ordered mesoporous materials and macromolecular building blocks. *Chem. Soc. Rev.* **2011**, *40*, 1107–1150. [[CrossRef](#)]
21. Wight, A.P.; Davis, M.E. Design and Preparation of Organic–Inorganic Hybrid Catalysts. *Chem. Rev.* **2002**, *102*, 3589–3614. [[CrossRef](#)]
22. Ahmed, M.; Sakthivel, A. Covalent grafting of cobalt carbonyl cluster on functionalized mesoporous SBA-15 molecular sieve and its applications towards hydroformylation of 1-octene. *J. Mol. Catal. A Chem.* **2016**, *424*, 85–90. [[CrossRef](#)]
23. Ren, Z.; Liu, Y.; Lyu, Y.; Song, X.; Zheng, C.; Feng, S.; Jiang, Z.; Ding, Y. Single-atom Rh based bipyridine framework porous organic polymer: A high active and superb stable catalyst for heterogeneous methanol carbonylation. *J. Catal.* **2019**, *369*, 249–256. [[CrossRef](#)]

24. Pilaski, M.; Artz, J.; Islam, H.-U.; Beale, A.M.; Palkovits, R. N-containing covalent organic frameworks as supports for rhodium as transition-metal catalysts in hydroformylation reactions. *Microporous Mesoporous Mater.* **2016**, *227*, 219–227. [[CrossRef](#)]
25. Arrigo, R.; Hävecker, M.; Schlögl, R.; Su, D.S. Dynamic surface rearrangement and thermal stability of nitrogen functional groups on carbon nanotubes. *Chem. Commun.* **2008**, 4891–4893. [[CrossRef](#)] [[PubMed](#)]
26. Liu, Z.; Du, Z.; Song, H.; Wang, C.; Subhan, F.; Xing, W.; Yan, Z. The fabrication of porous N-doped carbon from widely available urea formaldehyde resin for carbon dioxide adsorption. *J. Colloid Interface Sci.* **2014**, *416*, 124–132. [[CrossRef](#)] [[PubMed](#)]
27. Chen, M.; Shao, L.-L.; Dong, M.-Y.; Lv, X.-W.; Yuan, Z.-Y.; Qian, X.; Han, Y.-Y.; Ding, A.-X. Molecular-Level Synthesis of Cobalt Phosphide Nanocrystals Confined in Highly Nitrogen-Doped Mesoporous Carbon Electrocatalyst for Highly Efficient Dye-Sensitized Solar Cells. *ACS Sustain. Chem. Eng.* **2020**, *8*, 17245–17261. [[CrossRef](#)]
28. Bando, K.K.; Asakura, K.; Arakawa, H.; Isobe, K.; Iwasawa, Y. Surface Structures and Catalytic Hydroformylation Activities of Rh Dimers Attached on Various Inorganic Oxide Supports. *J. Phys. Chem.* **1996**, *100*, 13636–13645. [[CrossRef](#)]
29. Zhong, S. Study of the reactivity of chemisorbed CO on RhSiO<sub>2</sub> catalyst. *J. Catal.* **1986**, *100*, 270–274. [[CrossRef](#)]
30. Andersson, S.L.T.; Watters, K.L.; Howe, R.F. An XPS study of Rh<sub>6</sub>(CO)<sub>16</sub>-Al<sub>2</sub>O<sub>3</sub>. *J. Catal.* **1981**, *69*, 212–215. [[CrossRef](#)]
31. Carvalho, M.; Wieserman, L.F.; Hercules, D.M. Spectroscopic Characterization of Wilkinson's Catalyst Using X-ray Photoelectron Spectroscopy (ESCA). *Appl. Spectrosc.* **1982**, *36*, 290–296. [[CrossRef](#)]
32. Trzeciak, A.M.; Ziółkowski, J.J. Hydroformylation and isomerization reactions of hex-1-ene catalyzed by rhodium(I) complexes. *J. Mol. Catal.* **1988**, *43*, 335–341. [[CrossRef](#)]
33. Hou, C.; Zhao, G.; Ji, Y.; Niu, Z.; Wang, D.; Li, Y. Hydroformylation of alkenes over rhodium supported on the metal-organic framework ZIF-8. *Nano Res.* **2014**, *7*, 1364–1369. [[CrossRef](#)]
34. Huang, L.; Wu, J.C.; Kawi, S. Rh<sub>4</sub>(CO)<sub>12</sub>-derived functionalized MCM-41-tethered rhodium complexes: Preparation, characterization and catalysis for cyclohexene hydroformylation. *J. Mol. Catal. A Chem.* **2003**, *206*, 371–387. [[CrossRef](#)]
35. He, Y.; Chen, G.; Kawi, S.; Wong, S. Catalytic study of MCM-41 immobilized RhCl<sub>3</sub> for the hydroformylation of styrene. *J. Porous Mater.* **2009**, *16*, 721–729. [[CrossRef](#)]
36. Chen, J.; Qiao, L.; Zhou, Z.; Wu, X.; Guo, X.; Zong, S.; Ding, Y.; He, Y.; Yao, Y. Promoted Hydroformylation of Formaldehyde by Electronic Metal-Support Interactions in N-Group Functionalized Silica Supported Rhodium Catalyst. *Catal. Lett.* **2021**, *151*, 3664–3674. [[CrossRef](#)]
37. Nandi, M.; Mondal, P.; Islam, M.; Bhaumik, A. Highly Efficient Hydroformylation of 1-Hexene over an ortho-Metallated Rhodium(I) Complex Anchored on a 2D-Hexagonal Mesoporous Material. *Eur. J. Inorg. Chem.* **2011**, *2011*, 221–227. [[CrossRef](#)]
38. Shi, Y.; Lu, Y.; Ren, T.; Li, J.; Hu, Q.; Hu, X.; Zhu, B.; Huang, W. Rh Particles Supported on Sulfated g-C<sub>3</sub>N<sub>4</sub>: A Highly Efficient and Recyclable Heterogeneous Catalyst for Alkene Hydroformylation. *Catalysts* **2020**, *10*, 1359. [[CrossRef](#)]
39. Armarego, W.L.F. Chapter 3—Purification of Organic Chemicals. In *Purification of Laboratory Chemicals*, 8th ed.; Armarego, W.L.F., Ed.; Butterworth-Heinemann: Oxford, UK, 2017; pp. 95–634.

**Disclaimer/Publisher's Note:** The statements, opinions and data contained in all publications are solely those of the individual author(s) and contributor(s) and not of MDPI and/or the editor(s). MDPI and/or the editor(s) disclaim responsibility for any injury to people or property resulting from any ideas, methods, instructions or products referred to in the content.